On connectivity in the central nervous systeem : a magnetic resonance imaging study

Stieltjes, B.

MAGN RESON MED 2006 MAY; 55(5): 1124-31

— 10 —

Manganese-enhanced magnetic resonance imaging for *in vivo* assessment of damage and functional improvement following spinal cord injury in mice

B. Stieltjes, S. Klussmann, M. Bock, R. Umathun, J. Mangalathu, E. Letellier, W. Rittgen, L. Edler, P.H. Krammer, H.U. Kauczor, A. Martin-Villalba and M. Essig

In the past decades, much effort has been invested in developing therapies for spinal injuries. Lack of standardization of clinical read-out measures, however, makes direct comparison of experimental therapies difficult. Damage and therapeutic effects *in vivo* are routinely evaluated using rather subjective behavioural tests. Here we show that manganese-enhanced magnetic resonance imaging (MEMRI) can be used to examine the extent of damage following spinal cord injury (SCI) in mice *in vivo*. Injection of MnCl2 solution into the cerebrospinal fluid (CSF) leads to manganese uptake into the spinal cord. Furthermore, after injury MEMRI-derived quantitative measures correlate closely with clinical locomotor scores. Improved locomotion due to treating the detrimental effects of SCI with an established therapy (neutralization of CD95Ligand) is reflected in an increase of manganese uptake into the injured spinal cord. Therefore, we demonstrate that MEMRI is a sensitive and objective tool for *in vivo* visualization and quantification of damage and functional improvement after SCI. Thus, MEMRI can serve as a reproducible surrogate measure of the clinical status of the spinal cord in mice, potentially becoming a standard approach for evaluating experimental therapies.

Introduction

Traditionally, neuro-anatomical connections have been primarily studied in animals using degeneration methods[1] and anterograde/retrograde tracing techniques[2]. These techniques have two major disadvantages. First, animals need to be sacrificed for further processing for histology precluding longitudinal studies in the same subject. Second, these techniques yield structural information of connections but exclude the possibility of functional assessment.

Mn^{2+} is known to cause a shortening of the T_1 time of water protons in MRI leading to a strong contrast enhancement in T_1-weighted MRI[3]. Mn^{2+} is a divalent ion with chemical properties resembling Ca2+. It is actively transported into neurons via voltage-gated Ca^{2+} channels[4]. Generally, three major applications of MEMRI have developed[5]:

1 as a tissue contrast agent,
2 as a surrogate marker for neuronal cell activity and
3 for tracing of neuronal tracts.

First, after systemic $MnCl_2$ injection in rodents, specific uptake patterns of Mn^{2+} with enrichment within the grey matter of the brain were described[6,7]. Second, Mn^{2+} has been successfully used as a Ca^{2+} analogue to visualize activity-dependent uptake into the rat brain[3]. This has also been shown in songbirds, where an injection of MnCl2 solution into the cortex gave rise to a selective pattern of Mn^{2+} uptake in the brain[8]. Importantly, the amount of uptake was dependent on the level of neuronal activity[9]. Third, Pautler et al. were the first to exploit MEMRI for depicting neuronal connections. Injection of $MnCl_2$ solution into the vitreal chamber enabled visualization of the optical tract in mice[10]. Consecutively, multiple other uses have been described like intracranial $MnCl_2$ injection that resulted in the enhancement of several white matter tracts of the monkey brain[11]. Once inside an axon, Mn^{2+} is transported in both antero- and retrograde direction. Trans-synaptic propagation has also been observed[12].

In the last years the development of MRI techniques for *in vivo* examination of the injured spinal cord has been accelerated. Promising approaches using functional MRI in rodents have been

designed by different groups[13,14]. Similarly, diffusion anisotropy MRI has been applied for quantitative assessment of recovery following SCI in rats[15]. Very recently, the potential use of MEMRI to examine the axonal connectivity after SCI has been explored[16]. Nevertheless, the high intrinsic variability of these methods, although generally functional, renders them unsuitable for quantitative discrimination of minute differences in spinal cord integrity, especially in small animals like mice.

To date, no data is available on the *in vivo* visualization of the functional status of the mouse spinal cord using $MnCl_2$. We hypothesized that an intracerebroventricular (i.c.v.) injection of $MnCl_2$ would lead to spinal Mn^{2+} uptake with the amount of Mn^{2+} uptake into the spinal cord depending on its functional status. We tested this hypothesis in a mouse model of SCI, in which animals were treated with a therapy (neutralizing antibodies against CD95Ligand) that is neuroprotective and leads to axonal regeneration resulting in strong functional improvement[6,17]. Here, we show that MEMRI-derived parameters correlate closely with clinical scores of locomotor function. Therefore, MEMRI may serve as a sensitive *in vivo* method for monitoring neuronal activity and functionality within the spinal cord and, moreover, could provide an objective *in vivo* parameter for the evaluation of damage after SCI and treatment effects.

Materials and Methods

Spinal Cord Injury (SCI)

Animal experiments were approved by the German Cancer Research Center institutional animal care and use committee and the Regierungspräsidium Karlsruhe. For SCI, $MnCl_2$ injection and MRI scan animals were anesthetized using isoflurane. SCI was performed essentially as described before[17]. In brief, after laminectomy at the level Th 7/8 the dorsal 80% of the spinal cord were transected using fine irridectomy scissors leaving only the ventral funiculus intact. This procedure results in complete paraplegia directly after injury. Minor spontaneous recovery of hind limb function is usually observed in the consecutive weeks. In the double-blind therapy experiment, injured mice received saline solution or were treated with 50 μg neutralizing antibodies directed against CD95Ligand (MFL3; Pharmingen). Antibody and saline were injected intraperitoneally 30 min before SCI as well as twice weekly in the following 5 weeks.

Contrast Agent Injection

For i.c.v. injections anesthetized animals were mounted onto a stereotaxic frame. 0.25 μl 0.8 M $MnCl_2$ solution in saline were injected bilaterally into the lateral ventricles (coordinates: 1 mm caudal to the bregma, 1.5 mm lateral, 1.8 mm depth) using a microinjector (Harvard Apparatus). For cisterna magna injections, 0.5 μl 0.8 M $MnCl_2$ solution or 10 μl 0.5 M Gadolinium-DTPA solution (Magnevist, Schering), respectively, were injected using a 27 g needle attached to a microsyringe as described[18]. The $MnCl_2$ dose for intravenous (i.v.) application into the tail vein was 0.2 mmol/kg and 1 mmol/kg for subcutaneous (s.c.) administration.

Study Groups

The study was divided into several parts. In the first part, the time course experiment of Mn^{2+} uptake into the spinal cord, we performed an i.c.v. injection of $MnCl_2$ solution in one animal and measured the contrast enhancement in the spinal cord 0, 1, 2, 4, 8, 12, 24, 72 and 120 h afterwards. To evaluate alternative application routes, $MnCl_2$ solution was administered either i.v., s.c. or into the cisterna magna (n=2 per group). Imaging was performed 8 to 24 h after injection. In the second part, the comparison of contrast enhancement in the spinal cords of injured and uninjured mice, animals subjected to SCI (n=10) and uninjured controls (n=5) received $MnCl_2$ injections 5 weeks after SCI. MRI followed 60 h later. In the third part, the therapy experiment, $MnCl_2$ solution was injected into antibody-treated and control mice (n=6 per group) at 4 h and 5 weeks after SCI. Imaging was

always performed 60 h after injection. To examine the integrity of the CSF circulation system, Gadolinium-DTPA was injected into the cisterna magna of uninjured (n=2) and injured mice at 5 weeks after SCI (n=6). MRI followed at multiple time points between 5 min and 6 h after injection.

Behavioral Testing

All tests were performed in a double-blind manner. Spinal cord-injured mice were tested in the BBB locomotor and grid walk tests at 1, 2, 3, 4 and 5 weeks after injury. The BBB test was additionally performed after 1 day. All behavioral tests were recorded with a video camera. For assessing the overall locomotor performance the BBB locomotor rating scale was used with slight modifications[17,19]. The BBB scale is a standard measure for analyzing the open field locomotor performance of rats after SCI and grades the functional status of their limbs based on different aspects like joint movement, paw placement, weight support, coordination etc. Complete paraplegia results in a score of 0, while normally functional uninjured animals receive 21 points[19]. Deficits in descending motor control were examined using the grid walk test[17,20]. In this task the animals have to traverse a horizontal ladder-like grid that is elevated above the ground. To cross this runway animals have to place their limbs accurately on the irregularly spaced bars. The numbers of foot placement mistakes for 10 steps of each hind limb are counted and summed up. Uninjured mice usually make none or very few mistakes, whereas paraplegic animals are unable to step and therefore receive 20 error points.

MRI

MRI experiments were performed on a clinical 1.5 T scanner (SIEMENS Symphony, Erlangen, Germany) with a dedicated custom made animal volume resonator using a 3D-FLASH imaging pulse sequence with the following parameters. Mn^{2+} uptake time series experiment: TR = 35.0 ms, TE = 4.1 ms, flip angle = 70°, 60 partitions, partition thickness = 0.2 mm, FOV = 27 x 20 mm, matrix size = 128 x 96, voxel size = 0.2 x 0.2 x 0.2 mm, 22 averages. SCI and therapy experiments: TR = 14.0 ms, TE = 5.22 ms, flip angle = 30°, 28 partitions, partition thickness = 0.5 mm, FOV = 80 x 80 mm, matrix size = 512 x 512, voxel size = 0.15 x 0.15 mm, 32 averages. The experiments were performed in sagittal plane for positioning (3 averages) and in axial plane for detailed spinal cord imaging. Total imaging time was 60 minutes. Cisterna magna injection of $MnCl_2$ experiment: TR = 35.0 ms, TE = 4.1 ms, flip angle = 70°, 60 partitions, partition thickness = 0.2 mm, FOV = 51 x 29 mm, matrix size = 256 x 144, voxel size = 0.2 x 0.2 x 0.2 mm, 22 averages. Cisterna magna injection of Gadolinium-DTPA experiment: TR = 14.0 ms, TE = 5.22 ms, flip angle = 30°, 28 partitions, partition thickness = 0.5 mm, FOV = 80 x 80 mm, matrix size = 512 x 512, voxel size = 0.15 x 0.15 mm, 5 averages.

Data Processing and Statistics

Images were evaluated using the scanner software package (Syngo, SIEMENS, Erlangen, Germany). The spinal cord was outlined on axial slices and the mean signal was calculated. A second region of interest was placed outside the animal contours for noise measurement. Mean SNR and standard deviation (SD) were calculated for each slice. For the therapy experiment post-processing was performed by an observer blinded to the treatment. The signal to noise ratio (SNR) in the most proximal slice (figure 1c, position 3) was set to 100% and SNRs in consecutive slices scaled accordingly expressing relative SNR (%). The area under the curve (AUC) was calculated using the scanner software package (Syngo, SIEMENS, Erlangen, Germany). (The increase of Mn^{2+} uptake depending on the position was assessed by linear regression within the two groups. Correlations between MEMRI and behavioral tests were determined using Kendall's τ. BBB and grid walk scores in antibody-treated mice were compared to saline controls using the Wilcoxon rank sum test.

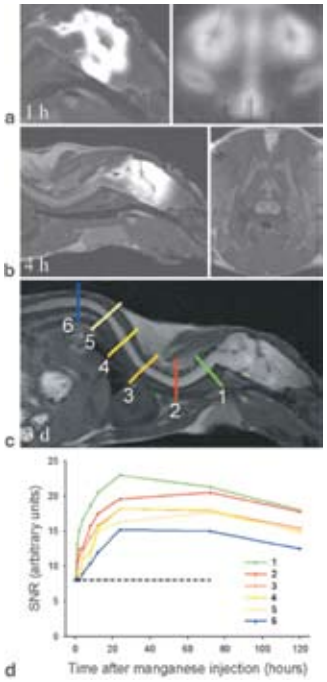

Figure 1 Contrast enhancement within the spinal cord after i.c.v.injection of MnCl2. (a) T1-weighted images in sagittal (left) and coronal orientation (right) at 1 h after injection. (b) Sagittal (left) and axial (right) T_1-weighted images at 4 h after injection. (c) Sagittal T1-weighted image showing homogeneous contrast enhancement within the spinal cord at 3 days after injection. (d) Time course of Mn2_ uptake at various levels of the spinal cord. The colored bars in (c) indicate the positions for the time course measurement corresponding to the following levels of the spinal cord: upper (1) and lower (2) cervical, upper (3), middle (4), and lower (5) thoracic, and upper (6) lumbar spinal cord. The dotted black line indicates baseline SNR.

Results

Intracerebroventricular $MnCl_2$ Injection Leads to Spinal Cord Enhancement

To test the suitability of an i.c.v. $MnCl_2$ solution injection for spinal cord imaging we measured the time course of Mn^{2+} enhancement after i.c.v. injection at various positions within the spinal cord. In the early time course, strong contrast enhancement was

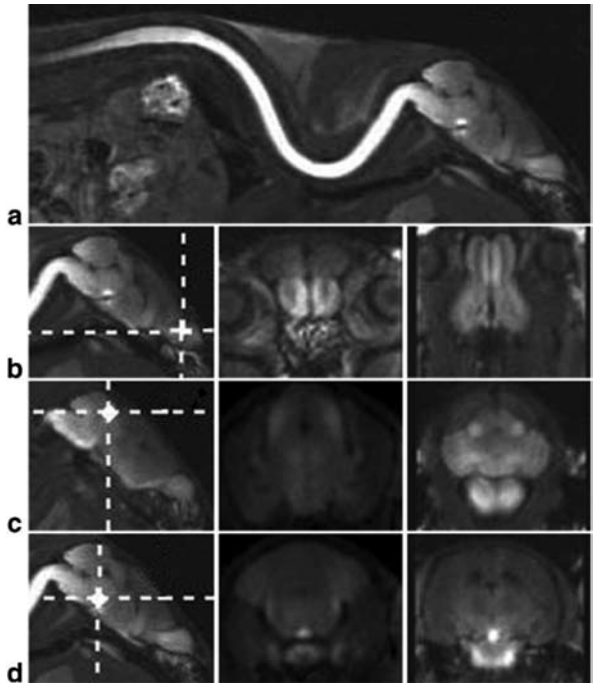

Figure 2 Injection of MnCl2 into the cisterna magna. (a) Sagittal T1-weighted image 24 h after injection into the cisterna magna. (b–d) From left to right sagittal, coronal and axial images at several levels in the brain. The level of the axial and coronal slices is indicated by the dotted white crosses on the sagittal images. Signal enhancement was observed in the rhinocortex (b), the colliculus superior (c), and the pituitary (d) as described previously (22). No significant Mn2- uptake in the motor cortex was observed.

observed in the motor cortex, along the ventricle walls and in both the ventral and the dorsal parts of the cervical spinal cord (figure 1a). Additionally, rapid transport over the CSF was noted with uptake both via the peri-spinal CSF as well as via the CSF within the central channel (figure 1b). Initially, Mn^{2+} was taken up into the spinal tissue directly adjacent to the figure but later the spinal cord showed homogenous Mn2+ distribution (figure 1c). The SNR within the spinal cord rose quickly in the first 24 h after injection. Afterwards, a plateau phase was reached that lasted another 48 h followed by a slow Mn^{2+} wash-out (figure 1d). This plateau reached different levels along the spinal cord with a clear

increase of SNR of two to three times baseline. Residual elevated signal intensity was present up to three weeks after injection, after which the SNR in the spinal cord returned to baseline. Direct injection of $MnCl_2$ solution into the cisterna magna gave rise to a rapid increase of signal primarily along the spinal cord suggesting a direct distribution of Mn^{2+} via the CSF (figure 2). Also, no uptake in the motor cortex was noted.

Concomitantly, we also tested the suitability of less invasive modes of $MnCl_2$ application. Systemic administration similarly leads to signal enhancement in the brain[6,21]. Mn^{2+} enters the brain primarily via the choroid plexus, from where it is distributed through the CSF into the parenchyma[6]. Thus, we examined Mn^{2+} uptake into the spinal cord after i.v. and s.c. application. The signal intensity within the spinal cord increased slightly, however, it was strongly reduced in comparison to the i.c.v. administration (data not shown), excluding such alternative routes of administration for examining the spinal cord.

Signal Enhancement is Reduced after SCI

After determining Mn^{2+} enhancement dynamics we tested the effect of SCI on Mn^{2+} uptake. We transected the dorsal 80% of the spinal cord at the level Th7/8, which led to paraplegia. $MnCl_2$ solution was injected five weeks after SCI and imaging performed 60 h later since at that time point a homogeneous Mn^{2+} uptake at the lesion level could be expected (figure 1d). Contrast enhancement in the spinal cord is shown for representative mice without (figure 3a) and with injury (figure 3b) in the sagittal plane. A clear interruption of contrast enhancement distal to the lesion in the injured mouse can be seen as shown in more detail on the axial slices (figure 3c). To quantify functional impairment we determined SNR within the spinal cord on MRI images measured perpendicular to the spinal cord surrounding the lesion site (figure 3d). Uninjured animals displayed a homogeneous SNR throughout the spinal cord (blue curve in figure 3d); after $MnCl_2$ injection a marked increase in SNR was noted (green). Rostral to the lesion, injured mice (red) showed a SNR comparable to non-

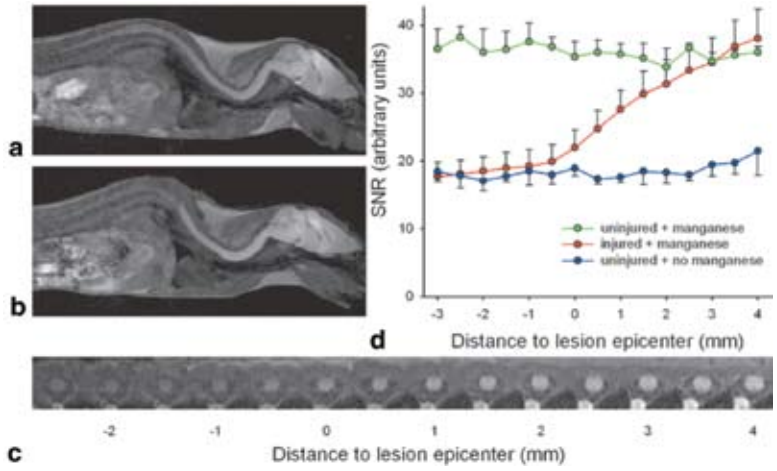

Figure 3 Visualization and quantification of SCI using MEMRI. (a) Continuous contrast enhancement throughout the spinal cord in an uninjured animal. (b) Clear interruption of contrast enhancement distal to the lesion site. Imaging was performed 60 h after SCI and $MnCl_2$ injection. (c) Axial slices of the injured mouse shown in (b). Note the decrease in contrast enhancement around the lesion epicenter. (d) SNR (+/-SD) in the spinal cord of uninjured mice with and without $MnCl_2$ injection (n = 5 per group) and injured mice (n = 10) 5 weeks after SCI. Distance in mm caudal (-) and rostral (+) to the lesion epicenter.

injured animals. Albeit moving further distal towards the lesion epicenter, the SNR gradually dropped approaching background levels at the lesion site and beyond. Thus, there is an injury-dependent reduction of Mn^{2+} uptake following SCI.

To examine whether the reduction of Mn^{2+} uptake is due to a compromised CSF circulation, we injected Gadolinium-DTPA into the cisterna magna of non-injured and SCI mice. Gadolinium-DTPA is a contrast agent that is mainly retained within the CSF[22,23]. In contrast to Mn^{2+}, Gadolinium-DTPA was in all cases detected within the CSF far beyond the site of the lesion, surrounding the lumbar spinal cord (figure 4). This excludes that the decreased Mn^{2+} uptake in injured mice is due to a compromised accessibility of the CSF to the spinal region caudal to the lesion.

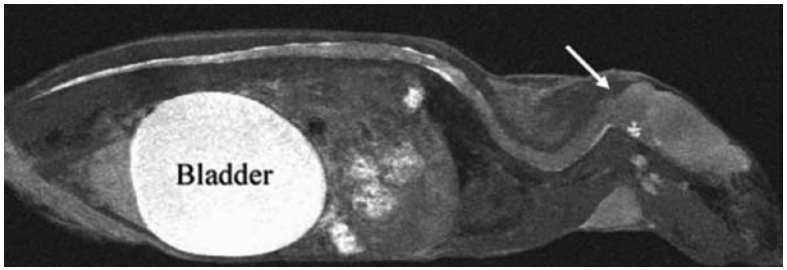

Figure 4 Gadolinium-DTPA injection into the cisterna magna of a spinal cord-injured mouse. Contrast is enhanced in the complete CSF, also caudal to the lesion epicenter. The arrow indicates the injection site.

Mn^{2+} Uptake Correlates with Functional Recovery following SCI

To test function-dependent Mn^{2+} uptake we performed MRI on mice treated with neutralizing antibodies directed against CD95Ligand and their saline-treated control counterparts. We have recently shown that this therapy protects neurons and oligodendrocytes from apoptotic cell death leading to enhanced axonal regeneration and improved functional recovery following SCI17. All animals were clinically tested once weekly using the BBB score[19] and a grid walk test[20]. In saline-treated animals minor signs of spontaneous locomotor function recovery were observed as shown before, whereas the anti-CD95Ligand antibody-treated mice improved significantly (figure 5)[17].

To evaluate therapy-induced changes in spinal Mn^{2+} uptake we performed the MEMRI experiment as described for the injured untreated animals. However, $MnCl_2$ solution was injected twice: at first at 4 h and for the second time at 5 weeks after SCI. Images were acquired 60 h later, and the SNR along the spinal cord was measured (figure 6a). We calculated the area under the curve (AUC) for both time points and tested the value of the change in AUC (Δ AUC) as a measure of clinical improvement. In saline-treated control animals Mn^{2+} uptake did not significantly increase with time (linear regression analysis of relative SNR (%) on the distance to the lesion epicenter: p = 0.018, slope -0.269, 95% confidence interval: -0.048 to -0.49, n=6). The relative SNR (%) at 3 d and at 5 weeks

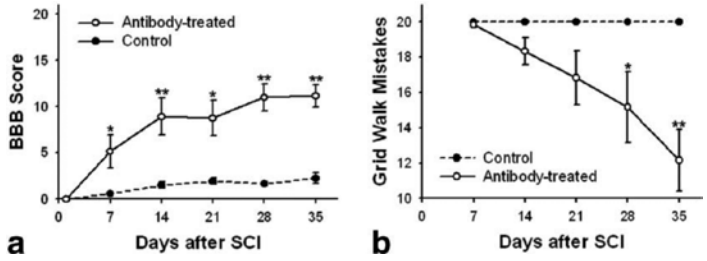

Figure 5 Clinical evaluation of motor function of antibody- and saline-treated mice following SCI. (a) BBB scores in antibody-treated (open circles) and untreated control (filled circles) animals (mean +/-SE; n = 6 per group). The overall locomotor performance significantly improved in the antibody-treated group, while only limited spontaneous recovery was observed in the saline control group (Wilcoxon rank sum test; *$p < 0.05$, **$p > 0.01$). (b) Number of grid walk mistakes in antibody-treated (open circles) and untreated control (filled circles) animals (mean +/-SE; n = 6 per group). The number of stepping mistakes significantly decreased in the treated group, while mice in the untreated control group did not regain the ability to step (Wilcoxon rank sum test; *$p < 0.05$, **$p > 0.01$).

after injury in a representative control animal is depicted in figure 6b together with the axial slices of the spinal cord of this mouse. In contrast, the anti-CD95Ligand antibody-treated animals showed a significant increase of Δ AUC (linear regression analysis: p = 0.0005, slope 1.150, 95% confidence interval: 0.831 to 1.470, n=6). In figure 6c the relative SNR (%) at 3 d and at 5 weeks after injury is shown for a representative treated animal. Importantly, at the early time point after SCI the MRI images of both groups were comparable. A gradual decrease of contrast enhancement along the rostro-caudal axis of the spinal cord was observed; reaching baseline levels at the lesion site, analogous to the curve of the injured untreated animals (compare figure 3). At the late time point, however, the images of treated and control mice differed strikingly. While in control animals the distribution of the Mn^{2+} signal had not changed in comparison to the early measurement, the contrast enhancement pattern was strongly changed in treated mice (figure 6c). Around and especially caudal to the lesion site the Mn^{2+} uptake was significantly increased, indicating preservation of active functional neurons at the level of injury and beyond. Yet, the SNR at and caudal to the lesion site never reached uninjured levels demonstrating residual damage despite treatment.

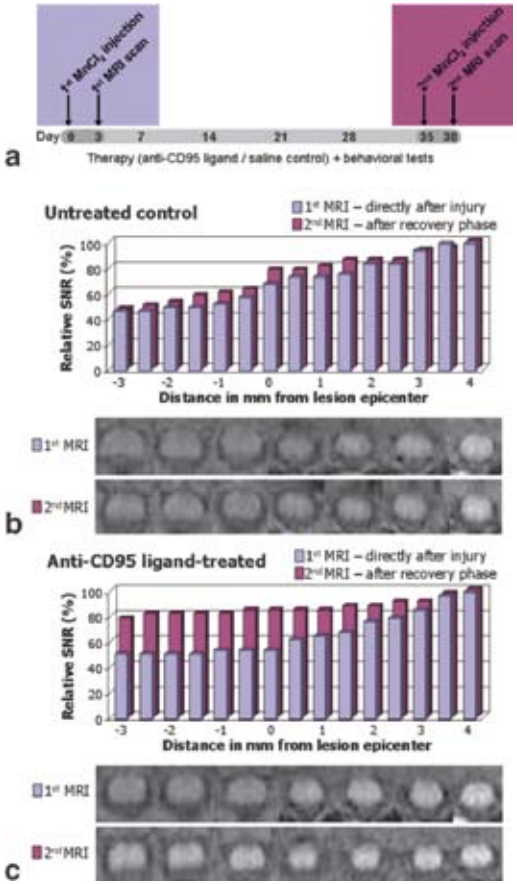

Figure 6 MEMRI for evaluation of therapy effects. (a) Schematic representation of the experiment. (b) Relative SNR (%) in the spinal cord directly after injury and 5 weeks later in a representative saline-treated animal. The axial slices depicted below were used for quantification. (c) Relative SNR (%) in a representative anti-CD95Ligand antibody-treated animal. Note the strong increase in contrast enhancement due to therapy.

The changes in Δ AUC between the early and late time points are plotted against the final behavioral test scores for both treated and control animals (figure 7). For testing the correlation of MEMRI with the clinical scores we ranked the 12 animals based on Δ AUC as well as on their behavioral test scores assuming that preservation of functional neurons is the cause for both increased

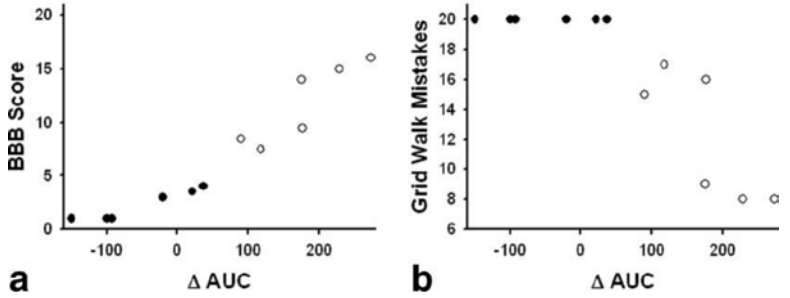

Figure 7 Correlation of MEMRI with behavioral tests for evaluation of therapy effects. The MEMRI-derived quantitative measure AUC for anti-CD95Ligand antibodytreated (open circles) and control mice (filled circles; n = 6 per group) is plotted against the clinical locomotor tests BBB score (a) and the number of mistakes in the grid walk test (b).

spinal Mn^{2+} uptake and improved motor function. A highly significant correlation between the two rankings was found (Kendall's $\tau = 0.9394$, $p = 0.000005$). Furthermore, the antibody- and saline-treated groups differed significantly with regard to MEMRI as well as BBB and grid walk ranks (Wilcoxon rank sum test; $p = 0.0011$). In conclusion, MEMRI-derived parameters correlate closely with the clinical status as evaluated using locomotor tests.

Discussion

The main problem in SCI is the interruption of neuronal connections and consecutive loss of neuronal tissue. Despite the general lack of optimism for functional recovery after SCI, in the past decade animal studies brought forward evidence for neuroprotection, axonal regeneration and consequent regain of locomotion and of some primitive forms of sensation after experimental therapy [24,25]. This has led to a great debate about the type and quality of evidence needed to select truly promising candidate therapies. In most animal studies the reported therapeutical success is based upon histological evidence and/or assessment of the overall locomotor activity (e.g. BBB score). Major disadvantages of these methods are the need to sacrifice the animals, the great

subjectivity and subsequent lack of standardization among the different laboratories. Here we developed an *in vivo* method for the evaluation of spinal cord function using MEMRI. This method has the important advantage of enabling a standardized and more objective follow-up of therapies over time.

The use of MEMRI for the functional assessment after SCI relies on the capacity of Mn^{2+} to mimic Ca^{2+}. Mn^{2+} is predominantly taken up by active neurons and less by the disconnected "electrically silent" ones. The rate of axonal Mn^{2+} transport described within the brain varies from 1.1 to 6.0 mm/h depending on injection volume and functional status of the neuronal tissue[26]. Signal propagation in our experiment was much faster than that calculated for axonal transport. Moreover, experiments have shown that a focal $MnCl_2$ injection into the motor cortex leads to uptake in the corticospinal tract with strong signal decay in the more distal regions of the corticospinal tract without detectable contrast enhancement beyond the midbrain level[26]. This indicates that in our setting visualization of the spinal cord using MEMRI is based on transport of Mn^{2+} via the CSF with local, activity-dependent uptake into the spinal cord. This hypothesis is strengthened by the experiment, in which $MnCl_2$ was injected directly into the cisterna magna. Here, we did not observe uptake in the motor cortex excluding a substantial role for active axonal Mn^{2+} transport via the corticospinal tract as a main route of contrast enhancement of the spinal cord. Instead, a strong contrast enhancement throughout the spinal cord resembling the contrast enhancement after an i.c.v. injection was evident. These findings are in accordance with a recent paper investigating i.p. application of $MnCl_2$ showing uptake only in selected areas of the brain (27). Altogether, our results indicate that MEMRI of the spinal cord after i.c.v. injection is primarily based on the CSF transport of Mn^{2+} and local activity-dependent uptake.

Injury to the spinal cord, especially in the transection model used here, may affect the integrity of CSF circulation[28]. Thus, it might be hypothesized that the near-background levels of Mn^{2+} uptake caudal to the lesion site found in mice directly after injury or in untreated mice five weeks after injury could be due to a block in CSF circulation. However, it is unlikely that the anti-CD95Ligand therapy acts on this level. Nevertheless, to exclude the possibility that our method merely depicts disruption of the CSF system, we injected Gadolinium-DTPA into the cisterna magna. In all injured and uninjured control mice the contrast agent passed beyond the level of the lesion site into the lumbar spinal cord to a comparable extent. These experiments indicate that transecting the dorsal 80% of the spinal cord – although inducing local damage to the CSF compartment – does not lead to a complete disruption of the CSF circulation. Thus, the specific contrast enhancement and lack of uptake caudal to the lesion site cannot be attributed to impeded CSF circulation.

A recent publication describes Mn^{2+} uptake in the hemi-sected spinal cord of rats after a local injection of $MnCl_2$ solution into the white matter of the spinal cord[16]. The authors discuss their findings exclusively in terms of axonal transport but their images reveal an even stronger Mn^{2+} uptake in the gray matter of the spinal cord than in the surrounding white matter, which indicates that in their experiments primary uptake by functional gray matter, as described in our setting, must also play a strong role. Moreover, in our experiments injection-induced trauma is minimized because an invasive and technically challenging focal injection into the white matter of the spinal cord requiring an additional laminectomy is not necessary. This is crucial for therapy monitoring since additional trauma to the spinal cord makes it more difficult to objectively determine therapy efficacy. Finally, the major advantage of our MEMRI approach is the possibility of quantitative assessment of damage and recovery.

An issue using Mn^{2+} for *in vivo* imaging is its neurotoxicity[29]. In contrast to focal injections into the brain parenchyma, an injection of $MnCl_2$ into the CSF has the advantage of rapid dilution of the toxic agent. Furthermore, in the experiments described here we stayed well within the limits of the known non-toxic dose[30]. Consequently, no alterations of vital or motor functions could be observed following i.c.v. $MnCl_2$ injection. Symptoms of manganism that resemble disorders described as extrapyramidal motor system dysfunction, which are typical for chronic Mn^{2+} exposure, did not develop[31].

Conclusion

We have devised a fast and safe *in vivo* method for visualization of the spinal cord and quantitative assessment of its functional status. Moreover, we demonstrated that MEMRI could substitute for behavioral tests or at least add to a more objective assessment of the spinal cord's functional status following SCI. This method could become a standard measurement for comparison of different therapies in different laboratories. MEMRI provides a surrogate read-out for damage and functional recovery after SCI. Finally, application of this method could be expanded to the study of other pathologies both in the CNS and the PNS.

Acknowledgements

This work was supported by the Christopher Reeve Paralysis Foundation (CRPF).

References

1 **Jones EG,** Powell TP. An anatomical study of converging sensory pathways within the cerebral cortex of the monkey. Brain 1970;93(4):793-820.

2 **Heimer L,** Robarts M. Neuroanatomical Tract-Tracing Methods. 1981. New York L, Plenum Press.

3 **Lin YJ,** Koretsky AP. Manganese ion enhances T1-weighted MRI during brain activation: an approach to direct imaging of brain function. Magn Reson Med 1997 Sep;38(3):378-88.

4 **Drapeau P,** Nachshen DA. Manganese fluxes and manganese-dependent neurotransmitter release in presynaptic nerve endings isolated from rat brain. J Physiol 1984 Mar;348:493-510.

5 **Koretsky AP,** Silva AC. Manganese-enhanced magnetic resonance imaging (MEMRI). NMR Biomed 2004 Dec;17(8):527-31.

6 **Aoki I,** Wu YJ, Silva AC, Lynch RM, Koretsky AP. *In vivo* detection of neuroarchitecture in the rodent brain using manganese-enhanced MRI. Neuroimage 2004 Jul;22(3):1046-59.

7 **Watanabe T,** Natt O, Boretius S, Frahm J, Michaelis T. *In vivo* 3D MRI staining of mouse brain after subcutaneous application of MnCl2. Magn Reson Med 2002 Nov;48(5):852-9.

8 **Van der Linden A,** Verhoye M, Van Meir V, Tindemans I, Eens M, Absil P, Balthazart J. *In vivo* manganese-enhanced magnetic resonance imaging reveals connections and functional properties of the songbird vocal control system. Neuroscience 2002;112(2):467-74.

9 **Tindemans I,** Verhoye M, Balthazart J, Van der Linden A. *In vivo* dynamic ME-MRI reveals differential functional responses of RA- and area X-projecting neurons in the HVC of canaries exposed to conspecific song. Eur J Neurosci 2003 Dec;18(12):3352-60.

10 **Pautler RG,** Silva AC, Koretsky AP. *In vivo* neuronal tract tracing using manganese-enhanced magnetic resonance imaging. Magn Reson Med 1998 Dec;40(5):740-8.

11 **Saleem KS,** Pauls JM, Augath M, Trinath T, Prause BA, Hashikawa T, Logothetis NK. Magnetic resonance imaging of neuronal connections in the macaque monkey. Neuron 2002 May;34(5):685-700.

12 **Pautler RG,** Mongeau R, Jacobs RE. *In vivo* trans-synaptic tract tracing from the murine striatum and amygdala utilizing manganese enhanced MRI (MEMRI). Magn Reson Med 2003 Jul;50(1):33-9.

13 **Spenger C,** Josephson A, Klason T, Hoehn M, Schwindt W, Ingvar M, Olson L.

Functional MRI at 4.7 tesla of the rat brain during electric stimulation of forepaw, hindpaw, or tail in single- and multislice experiments. Exp Neurol 2000 Dec;166(2): 246-53.

14 **Lawrence J,** Stroman PW, Bascaramurty S, Jordan LM, Malisza KL. Correlation of functional activation in the rat spinal cord with neuronal activation detected by immunohistochemistry. Neuroimage 2004 Aug;22(4):1802-7.

15 **Nevo U,** Hauben E, Yoles E, Agranov E, Akselrod S, Schwartz M, Neeman M. Diffusion anisotropy MRI for quantitative assessment of recovery in injured rat spinal cord. Magn Reson Med 2001 Jan;45(1):1-9.

16 **Bilgen M,** Dancause N, Al Hafez B, He YY, Malone TM. Manganese-enhanced MRI of rat spinal cord injury. Magn Reson Imaging 2005 Sep;23(7):829-32.

17 **Demjen D,** Klussmann S, Kleber S, Zuliani C, Stieltjes B, Metzger C, Hirt UA, Walczak H, Falk W, Essig M, Edler L, Krammer PH, Martin-Villalba A. Neutralization of CD95 ligand promotes regeneration and functional recovery after spinal cord injury. Nat Med 2004 Apr;10(4):389-95.

18 **Furlan R,** Pluchino S, Marconi PC, Martino G. Cytokine gene delivery into the central nervous system using intrathecally injected nonreplicative viral vectors. Methods Mol Biol 2003;215:279-89.

19 **Basso DM,** Beattie MS, Bresnahan JC. A sensitive and reliable locomotor rating scale for open field testing in rats. J Neurotrauma 1995 Feb;12(1):1-21.

20 **Metz GA,** Merkler D, Dietz V, Schwab ME, Fouad K. Efficient testing of motor function in spinal cord injured rats. Brain Res 2000 Nov;883(2):165-77.

21 **Kuo YT,** Herlihy AH, So P W, Bhakoo KK, Bell JD. *In vivo* measurements of T1 relaxation times in mouse brain associated with different modes of systemic administration of manganese chloride. J Magn Reson Imaging 2005 Apr;21(4):334-9.

22 **Liu CH,** D'Arceuil HE, de Crespigny AJ. Direct CSF injection of MnCl(2) for dynamic manganese-enhanced MRI. Magn Reson Med 2004 May;51(5):978-87.

23 **Wan XM,** Fu TC, Smith PH, Brainard JR, London RE. Magnetic resonance imaging study of the rat cerebral ventricular system utilizing intracerebrally administered contrast agents. Magn Reson Med 1991 Sep;21(1):97-106.

24 **Klussmann S,** Martin-Villalba A. Molecular targets in spinal cord injury. J Mol Med 2005 Sep;83(9):657-71.

25 **Schwab ME.** Increasing plasticity and functional recovery of the lesioned spinal cord. Prog Brain Res 2002;137:351-9.

26 **Leergaard TB,** Bjaalie JG, Devor A, Wald LL, Dale AM. *In vivo* tracing of major rat brain pathways using manganese-enhanced magnetic resonance imaging and three-dimensional digital atlasing. Neuroimage 2003 Nov;20(3):1591-600.

27 **Yu, X,** Wadghiri, YZ, Sanes, DH, Turnbull, DH. *In vivo* auditory brain mapping in mice with Mn-enhanced MRI. Nat Neurosci. 2005 Jul; 8(7):961-8

28 **Falcone S,** Quencer RM, Green BA, Patchen SJ, Post MJ. Progressive posttraumatic myelomalacic myelopathy: imaging and clinical features. AJNR Am J Neuroradiol 1994 Apr;15(4):747-54.

29 **Keen CL,** Ensunsa JL, Clegg MS. Manganese metabolism in animals and humans including the toxicity of manganese. Manganese and its Role in Biological Processes. 2000. New York, Marcel Dekker.

30 **Crossgrove J,** Zheng W. Manganese toxicity upon overexposure. NMR Biomed 2004 Nov;17(8):544-53.

31 **Donaldson J.** The physiopathologic significance of manganese in brain: its relation to schizophrenia and neurodegenerative disorders. Neurotoxicology 1987;8(3):451-62